



Synthesis, induced-fit docking investigations, and in vitro aldose reductase inhibitory activity of non-carboxylic acid containing 2,4-thiazolidinedione derivatives

Rosanna Maccari^{a,*}, Rosaria Ottanà^a, Rosella Ciurleo^a, Dietmar Rakowitz^b, Barbara Matuszczak^b, Christian Laggner^c, Thierry Langer^c

^a Dipartimento Farmaco-chimico, Facoltà di Farmacia, Università di Messina, Polo Universitario dell'Annunziata, 98168 Messina, Italy

^b Department of Pharmaceutical Chemistry, Institute of Pharmacy, University of Innsbruck, Innrain 52a, A-6020 Innsbruck, Austria

^c Department of Pharmaceutical Chemistry, Institute of Pharmacy and Centre for Molecular Biosciences (CMBI), University of Innsbruck, Innrain 52c, A-6020 Innsbruck, Austria

ARTICLE INFO

Article history:

Received 15 February 2008

Revised 23 April 2008

Accepted 30 April 2008

Available online 3 May 2008

Keywords:

2,4-Thiazolidinediones

Aldose reductase

Diabetes mellitus

Induced-fit docking

ABSTRACT

In continuation of our studies, we here report a series of non-carboxylic acid containing 2,4-thiazolidinedione derivatives, analogues of previously synthesized carboxylic acids which we had found to be very active in vitro aldose reductase (ALR2) inhibitors. Although the replacement of the carboxylic group with the carboxamide or *N*-hydroxycarboxamide one decreased the in vitro ALR2 inhibitory effect, this led to the identification of mainly non-ionized derivatives with micromolar ALR2 affinity. The 5-arylidene moiety deeply influenced the activity of these 2,4-thiazolidinediones. Our induced-fit docking studies suggested that 5-(4-hydroxybenzylidene)-substituted derivatives may bind the polar recognition region of the ALR2 active site by means of the deprotonated phenol group, while their acetic chain and carbonyl group at position 2 of the thiazolidinedione ring form a tight net of hydrogen bonds with amino acid residues of the lipophilic specificity pocket of the enzyme.

© 2008 Elsevier Ltd. All rights reserved.

1. Introduction

Diabetes mellitus (DM) is a common chronic metabolic disease, which is always associated with severe degenerative complications, such as neuropathy, nephropathy, retinopathy, cataracts, accelerated atherosclerosis, increased risk of myocardial infarction and stroke. The onset of these pathologies is a dramatic event in the course of both type 1 and type 2 diabetes (DM1 and DM2). In fact, their prevention and control are still serious and challenging therapeutic problems as they represent the leading causes of morbidity and mortality for diabetic patients.^{1–3}

Prolonged exposure to high concentrations of glucose is the main factor responsible for the pathogenesis of secondary diabetic complications. According to several predominant theories, this occurs through a variety of metabolic mechanisms, such as increased intracellular formation of advanced glycation-end products, abnormal activation of protein kinase C, increased flux of glucose through both the polyol and the hexosamine pathways, which lead to microvascular and macrovascular damage in the long run.^{3–5} It has been demonstrated that careful control of glycaemia can delay the emergence of these harmful effects.^{1,6} However, the onset of

long-term complications is unavoidable, since glycaemic levels cannot be completely normalized in individuals with diabetes. In addition, in many patients affected by DM2, vascular complications are already present at the time of diagnosis.³

The worldwide incidence of DM is very high and it is predicted to rise from the current estimate of about 180 million to more than 360 million by 2030.⁷ Currently, there are few drugs that are able to counteract the development of the associated pathologies. Therefore, the need to search for new drug candidates in this field appears to be critical.

The increased flux of glucose through the polyol pathway, which occurs under conditions of hyperglycaemia in tissues possessing insulin-independent glucose transport (retina, lenses, kidney, and nerve), is a well-known factor implicated in the development of secondary diabetic complications.^{4,8–10}

Aldose reductase (EC 1.1.1.21, ALR2), a member of the aldo-keto reductase superfamily, is the first and rate-limiting enzyme of the polyol pathway. It catalyzes the NADPH-dependent reduction of glucose to sorbitol which, in some tissues, is oxidized to fructose by sorbitol dehydrogenase.

Under euglycaemic conditions, ALR2, which has low affinity for glucose, produces little sorbitol. Indeed, a wide variety of aldehydes, especially medium-chain hydrophobic lipid-derived aldehydes and their glutathione adducts, are reduced more efficiently

* Corresponding author. Tel.: +39 90 6766406; fax: +39 90 355613.

E-mail address: rmaccari@pharma.unime.it (R. Maccari).

than glucose by ALR2. This would suggest that the most common role of ALR2 may be the removal of potentially toxic aldehydes generated during lipid peroxidation.^{9,11}

In contrast, under hyperglycaemic conditions, an excess of glucose (more than 30% of the total metabolized amount) is converted to sorbitol through the polyol pathway in tissues possessing insulin-independent uptake of glucose, leading to intracellular accumulation of this osmotically active polyol. At the same time, NADPH and NAD⁺ deprivation causes changes in cellular redox potentials, increased oxidative stress and reduced activity of other NADPH-dependent enzymes, such as nitric oxide (NO) synthase and glutathione reductase.⁹ Alterations of cytokine signalling and kinase cascades are also involved.^{4,9,12–14} These metabolic and biochemical changes result in inflammation, chronic vascular damage and decrease in nerve conduction velocity, and have been recognized as being related to the pathogenesis of diabetic complications.^{4,8,12–15}

Therefore, ALR2 inhibition has been proposed as a pharmacological strategy to prevent or delay the onset and progression of such pathologies, independently of glycaemia control.

In addition, other possible therapeutical applications of ALR2 inhibitors (ARIs) are currently emerging. In fact, recent studies have suggested that ALR2 may be involved in several physiological cellular functions, including growth and signalling.^{9,12} In particular, it has been demonstrated that ALR2 inhibition can suppress the lipopolysaccharide-induced production of pro-inflammatory cytokines, such as TNF- α , IL-6, IL-1 β , IFN- γ and inflammatory mediators, such as NO and prostaglandin E₂ (PGE₂) in macrophages.¹³ TNF- α -induced overexpression of cyclooxygenase 2 together with PGE₂ production have also been prevented in human colon cancer cells.¹⁶ As a consequence, ALR2 inhibition could be a novel approach to the chemoprevention of colon cancer as well as to the therapeutic treatment of diseases associated with high levels of cytokine expression, such as inflammation, rheumatoid arthritis and sepsis.^{9,13,16}

Although numerous ARIs have been reported over the last three decades,^{14,17–20} many of them proved to be clinically inadequate, because of pharmacokinetic problems, low efficacy or adverse side-effects. Currently, epalrestat (Fig. 1) is the only ARI available on the market²¹ and few molecules (such as fidaostat, Fig. 1) are in late-stage clinical development.^{19,22}

In particular, two main classes of orally active ARIs have been identified so far: cyclic imides, mostly hydantoin (such as sorbinil, fidaostat; Fig. 1) and carboxylic acids (such as zopolrestat, epalrestat; Fig. 1).^{14,17–20} In addition, 2,4-thiazolidinediones (2,4-TZDs) have received attention as hydantoin bioisosteres that are potentially devoid of hypersensitivity reactions apparently related to the hydantoin ring. In fact, many 2,4-TZDs have been reported as both antihyperglycaemic agents and ARIs, especially after the discovery of 2,4-thiazolidinedione derivatives as oral antidiabetic drugs.^{14,17–20}

In the last few years, we have synthesised numerous 5-arylidene-2,4-thiazolidinediones (**1–3**, Fig. 1) which were designed and assayed as *in vitro* ARIs.^{23–25} They possess the structural requisites considered critical for ALR2 inhibition: (a) an acidic function and/or H-bond acceptor groups that are able to interact with a positively charged recognition region of the ALR2 active site formed by Tyr48, His110, Trp111 and the nicotinamide ring of the cofactor NADP⁺ and (b) an aromatic moiety, which can establish hydrophobic interactions with a lipophilic pocket of the enzyme lined by Leu300 and Trp111.^{17–20,26–28} In addition, molecular docking simulations into the ALR2 active site highlighted that phenolic or carboxylic groups in the 5-benzylidene moiety can favourably interact either with amino acid residues lining this lipophilic pocket, such as Leu300, or with the positively charged recognition region.²⁵

Most 2,4-TZDs **1–3** are effective *in vitro* ARIs, with micromolar or submicromolar IC₅₀ values.^{23–25} The biological data we have collected so far have shown that the presence of an acetic chain on N-3 (compounds **3**) is related to the highest inhibition levels.

N-unsubstituted analogues **1** were also shown to be good ALR2 inhibitors. However, they were always less potent (from 10 to 100 times) than the corresponding acids **3**. In addition, analogous methyl esters **2**, although devoid of any acidic functionality, were shown to satisfy the minimal requisites for ALR2 inhibition, that is, the formation of hydrogen bonds with Tyr48 and His110 and the presence of a lipophilic aromatic moiety. In fact, some of them produced appreciable inhibition levels, similar to those of N-unsubstituted 2,4-TZDs **1**.^{23,24}

In continuing our search aimed at identifying new active analogues, we designed the synthesis of non-carboxylic acid containing 5-arylidene-2,4-thiazolidinedione derivatives.

Indeed, carboxylic acids that are active as ARIs are potent *in vitro* inhibitors. However, their effectiveness generally decreases *in vivo*, probably because of their poor capability to penetrate key target tissues, in particular peripheral nerves.^{17,19,20} Thus, the development of new low acidity ARIs, with pK_a values higher than those of carboxylic acids, is desirable because they may display better bioavailability than their carboxylic acid counterparts.

In particular, we replaced the carboxylic acetic chain on N-3 of (5-arylidene-2,4-dioxothiazolidin-3-yl)acetic acids (**3**) with the isostere acetamide and *N*-hydroxyacetamide moieties, obtaining (5-arylidene-2,4-dioxothiazolidin-3-yl)acetamides (**4**) and the analogous *N*-hydroxyacetamides (**5**), respectively (Fig. 2). They fitted the pharmacophoric model which we had previously defined for 5-arylidene-2,4-thiazolidinediones effective as ARIs, consisting of two H-acceptor groups and a lipophilic region.²⁴

Our initial hypothesis was that the acetamide group of compounds **4** might be able to bind the ALR2 active site via hydrogen bonds, analogously to the acetate chain of esters **3**.

On the other hand, the *N*-hydroxycarboxamide moiety (compounds **5**) can mimic monoanionic acidic groups. In addition, it is known that it can serve as both hydrogen bond donor and acceptor, as well as a metal chelating moiety,²⁹ thereby playing an important role in a variety of biologically active compounds.³⁰

The substitution pattern of the 5-arylidene moiety of 2,4-TZDs **4** and **5** was based on the previously acquired SARs. The presence of an additional aromatic ring or an H-bond donor group in this moiety was shown to enhance the ALR2 inhibitory effect.^{23–25}

We here report the synthesis and *in vitro* ALR2 inhibitory activity of a series of 5-arylidene-2,4-thiazolidinediones **4** and **5**. Additionally, induced-fit docking (IFD) studies were carried out in order to gain new insight concerning the possible binding modes of our compounds, which should also be useful to guide the future synthesis of improved compounds. Furthermore, it should serve as an evaluation of the scope and limitations of the IFD method.

2. Chemistry

(*Z*)-(5-Arylidene-2,4-dioxothiazolidin-3-yl)acetamides (**4a–g**) were prepared by the reaction of the corresponding (*Z*)-5-arylidene-2,4-thiazolidinediones (**1**), synthesised according to a reported procedure,^{23,24} with 2-chloroacetamide in refluxing acetonitrile, in the presence of potassium carbonate (Scheme 1). The synthesis of hydroxybenzylidene-substituted acetamides **4h–k** was carried out by adding 2-chloroacetamide dropwise to a solution of corresponding 2,4-TZDs **1** and potassium carbonate in acetonitrile over 2 h, in order to prevent the nucleophilic attack of hydroxyl group to chloroacetamide.

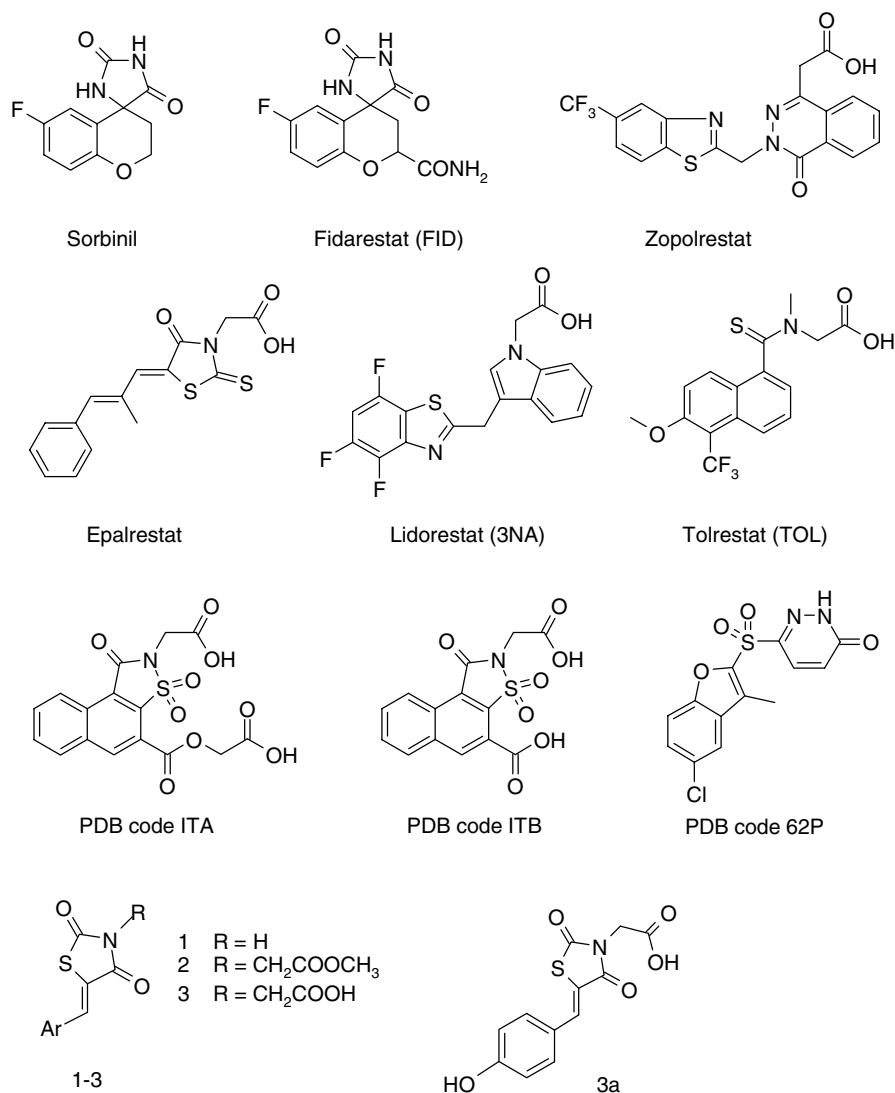


Figure 1. Chemical structures of some ARIs.

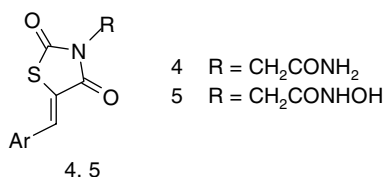


Figure 2. General structure of derivatives 4 and 5.

In the synthesis of (*Z*)-(5-arylidene-2,4-dioxothiazolidin-3-yl)-*N*-hydroxyacetamides (**5**) we applied a procedure reported by Reddy et al.³¹ The treatment of acids **3** with ethylchloroformate in diethylether, in the presence of triethylamine, followed by the addition of a freshly prepared solution of hydroxylamine in methanol, provided the desired compounds **5** (Scheme 1). The starting (*Z*)-(5-arylidene-2,4-dioxothiazolidin-3-yl)acetic acids (**3**) were synthesised by the treatment of (*Z*)-2,4-TZDs **1** with methyl bromoacetate, using potassium carbonate as base, and subsequent hydrolysis of methyl esters **2** in acidic medium, as already reported (Scheme 1).²⁴

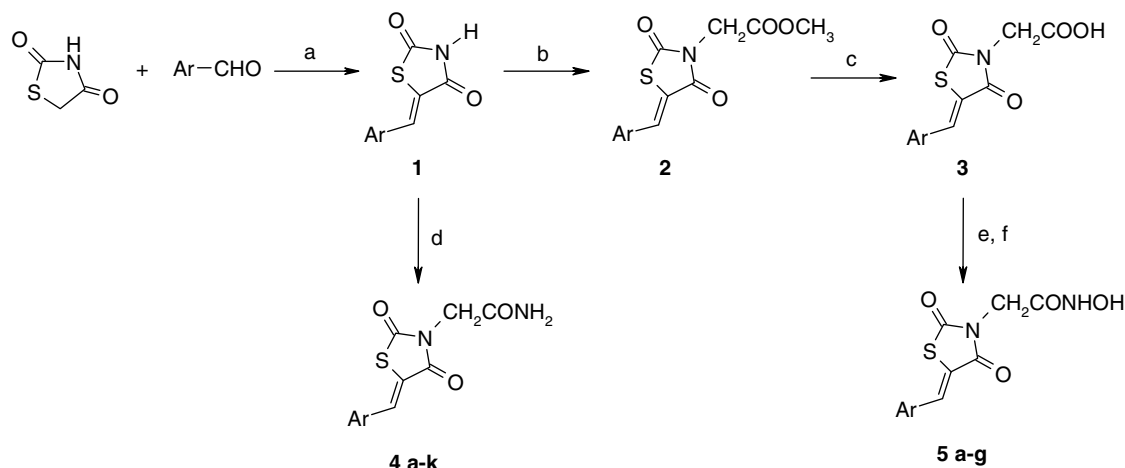
In an attempt to increase the yields of *N*-hydroxyacetamides **5** (30–50%) and to reduce reaction times (24–40 h), we carried out the same synthesis by irradiation with microwaves (MW). Upon

MW-irradiation, the treatment of acids **3** with ethylchloroformate and the subsequent reaction of the intermediate anhydrides with hydroxylamine produced compounds **5** in overall ten minutes and in 40–65% yields. This MW-assisted procedure allowed a marked decrease in the reaction times and a 10–15% increase in yields and thus provided a very rapid and convenient method to prepare *N*-hydroxyacetamides **5**.

The structures of compounds **4** and **5** were assigned on the basis of their analytical and spectroscopic data.

The ¹H NMR spectra of compounds **4** showed a singlet at 4.19–4.27 ppm, due to the resonance of the methylene group of the acetamide chain on N-3, which was diagnostic. Their ¹³C NMR spectra showed a triplet at 43.3–44.0 ppm and a singlet at 165.3–166.2 ppm, attributable to the methylene group and to the carbonyl group of the acetamide chain, respectively, which contributed to the unambiguous assignment of their structure.

¹H NMR spectra of *N*-hydroxyacetamides **5** displayed a singlet at 4.19–4.63 ppm, due to the resonance of the methylene group on N-3, and two broad singlets, exchangeable with D₂O, in the range from 9.01 to 11.0 ppm, attributable to the resonance of the NHOH group protons. In ¹³C NMR spectra, the methylene group on N-3 resonated at 41.5–46.2 ppm; in addition, the carbonyl groups of the thiazolidinedione ring and of the *N*-hydroxyacetamide chain resonated in the range between 162.5 and 168.6 ppm.



Scheme 1. Reagents and conditions: (a) $C_5H_{11}N$, C_2H_5OH , Δ ; (b) $BrCH_2COOCH_3$, K_2CO_3 , acetone; (c) $AcOH$, HCl , Δ ; (d) $ClCH_2CONH_2$, K_2CO_3 , CH_3CN , Δ ; (e) $ClCOOC_2H_5$, $(C_2H_5)_3N$, diethyl ether, MW (max 300 W) $80^\circ C$; (f) NH_2OH , CH_3OH , MW (max 300 W) $80^\circ C$.

The monitoring of the course of the reaction of acids **3** with ethylchloroformate, by means of 1H NMR spectra, also enabled the intermediate anhydrides to be identified. A singlet at 4.60 ppm was attributable to the resonance of the methylene group of the acetic chain on N-3, slightly more deshielded than the corresponding group of starting acids **3**, whereas a quartet at circa 4.40 ppm and a triplet at 1.40 ppm were due to the resonance of the ethyl group of the anhydride.

3. Induced-fit docking

Over the last few years, many X-ray crystal structures of ALR2 have been deposited in the PDB database.³² Experimental data showed that the ALR2 binding site can be divided into two sub-pockets, a catalytic pocket (also called the recognition region) and a specificity pocket. The catalytic pocket contains one molecule of $NADP^+$ and is usually occupied by an acidic moiety of the bound ligand. Its conformation is rather stable in all the various reported crystal structures. In contrast, the specificity pocket can adopt different conformations, adapting itself to the size of the bound ligands via movement of the loop region between Cys298 and Cys303 and the different rotameric states of the surrounding amino acid side chains, especially of Leu300 which acts as a gate-keeper between the closed and open states. Until recently, only three distinct conformations of the specificity pocket were known, and were called by Zentgraf et al. as the 'sorbiniil conformation', the 'tolrestat conformation' and the 'IDD594 conformation'.³³ The three different binding pocket conformations are shown in Figure 3, as exemplified by the three PDB structures 1PWM (ligand fidarestat, Fig. 1, sorbiniil conformation),³⁴ 2FZD (ligand tolrestat, Fig. 1, tolrestat conformation),³⁵ and 1Z3N (ligand lidorestat, Fig. 1, IDD594 conformation)³⁶ that were used in this study. The same authors reported two novel binding modes observed for two different naphtho[1,2-*d*]isothiazole acetic acid derivatives (ITA and ITB, Fig. 1) exemplified by the structures with PDB codes 2NVC and 2NVD.^{33,37} While the ligands are found in different regions, the overall conformation of the protein (especially the specificity pocket) is similar to that of the sorbiniil conformation (Fig. 3). The most distinct differences are the rotation of Trp20 and the subsequent breaking of the salt bridge between Lys21 and a $NADP^+$ phosphate group in 2NVD.

As stated above, the ALR2 binding site shows a high degree of flexibility, which poses a big challenge to those trying to

investigate possible binding modes of a given ligand. This problem has been thoroughly discussed in a recent paper given by Zentgraf et al.³³ One of the lessons learned from their studies is that the attempt to predict the possible binding mode of a given ligand by simply comparing its substructure to those of compounds with experimentally determined binding modes can often fail, even amongst compounds that are structurally closely related. The results from high-resolution X-ray crystal structures suggest that both the hydantoin-based ALR2 inhibitors such as sorbiniil, which have a pK_a of about 8.0, and a recently reported sulfonyl-pyridazinone derivative (Fig. 1, PDB code 62P, complexes 1Z89 and 1Z8A), which has a calculated pK_a of about 9.3, are deprotonated at the binding site.³⁸ This deprotonated state may be stabilized by the nearby positive charges at $NADP^+$ and Lys77, as well as by the hydrogen bonds donated by Trp111 and His110. Based on these results, we expect that our *N*-hydroxyacetamides **5**, which have calculated pK_a values of about 8.7,³⁹ are also binding in their deprotonated form, which was supported by more conclusive poses as well as lower docking score values in multiple docking runs (details not shown).

One method that tries to overcome binding site flexibility during docking is the IFD protocol developed by Schrödinger, LLC.⁴⁰ This method has already been successfully used to cross-dock tolrestat into the binding site of 2ACR, which corresponds to the closed sorbiniil conformation.⁴⁰ However, Zentgraf et al. reported that they were not able to predict the correct binding modes of their naphtho[1,2-*d*]isothiazole acetic acid derivatives using the induced-fit methodology.³³

We chose to evaluate the IFD method to see how well this method is able both to reproduce known binding conformations and to predict new ones presented with different protein geometries, to give possible explanations for the SARs and possible binding modes of our compounds. With an ideal IFD protocol, one could expect that, no matter which experimental structure is used as an input geometry for the docking, the correct conformations of both the ligand and the protein would always be found. Previous studies, however, showed that this is not the case. In the studies of Sherman et al.⁴⁰ three residues whose side-chains should be regarded as flexible during the IFD process were manually selected for the ALR2 example. One may argue, of course, that the knowledge about which side-chains have to move was already available. In the case of ALR2, there are many different flexible side chains surrounding the binding site, so that we would have to include about five or six of them to sample all the movements we know to take place amongst the dif-

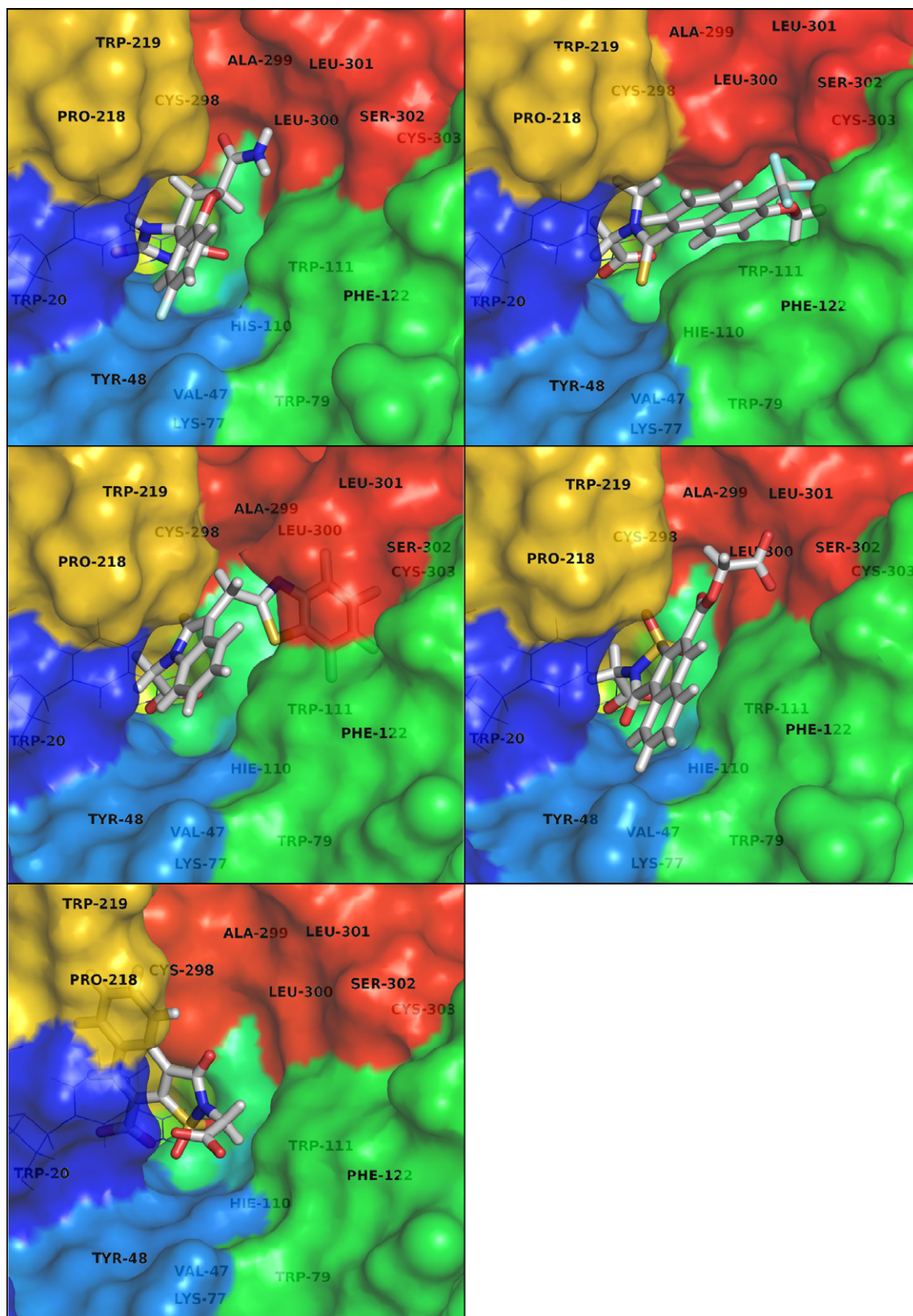


Figure 3. Comparison of different binding modes reported for ALR2 protein–ligand complexes, exemplified by the complexes used in this study. Graphics were created with PyMOL.⁴⁶ *Top left:* 1PWW (ligand fidarestat, ‘sorbinil conformation’),³⁴ *top right:* 2FZD (ligand tolrestat, ‘tolrestat conformation’),³⁵ *middle left:* 1Z3N (ligand lidorestat, ‘IDD594 conformation’),³⁶ *middle right:* 2NVC (ligand code ITA),³⁷ *bottom left:* 2NVD (ligand code ITB).³⁷ The important neighboring amino acids are labelled; the labels of groups lying further in the back have lower contrast. The cofactor NADP, placed behind the ligands in this view, is represented in line-mode.

ferent experimental structures. This would, of course, enlarge the binding site and thus increase the chance of the ligands being

wrongly placed along the pocket walls. However, we had representative examples for five different binding site conformations

available, and we knew that Leu300 exhibits the biggest contribution to the flexibility of the binding site. We thus decided to perform IFD into these different binding site geometries with a few selected ligands, together with the native ligands of all the selected protein ligand complexes, mutating only Leu300 during the initial docking run. The native ligands were used for cross-docking comparison, to see how well the different starting structures could transform into the different geometries and thus accommodate the ligands of the other structures in a conformation similar to their experimentally determined ones. We also wanted to use the results from these compounds as a guideline to decide whether there is a measure that is an indicator of the correct binding mode, for example, a lower GlideScore value.

We selected the complexes 1PWM, 2FZD, 1Z3N, 2NVC and 2NVD, which are all derived from human ALR2 and have a high experimental resolution (0.92, 1.08, 1.04, 1.65 and 1.55 Å, respectively).

The ligands we chose for docking were the corresponding ligands fidarestat, tolrestat, lidorestat, the compounds with the PDB codes ITA and ITB, and six compounds selected from our own 2,4-TZDs: **3a**, **4g**, **4i**, **5b**, **5e**, and **5g**. Compounds **4g** and **4i** were chosen as representatives for the acetamides **4**; **4g** is a close yet inactive derivative of **4i** which, in turn, is the most effective out of the acetamides **4**, **5b**, **5e** and **5g** are different examples of the *N*-hydroxyacetamides which all show high ALR2 affinity, yet bear aromatic residues of different shapes, sizes and polarities; finally, compound **3a** (Fig. 1, IC₅₀ = 0.15 μM, previously reported by us)²⁴ was included as an acetic acid derivative bearing the same aromatic residue as **4i** and **5g**.

The selected PDB structures were processed in Maestro (Schrödinger, LLC)⁴¹ using the Protein Preparation Wizard.

Since our compounds are assayed with ALR2 from bovine lenses, we also made a homology model using the Structure Prediction tool of Prime accessible from the Maestro GUI. The sequence of ALR2 from *Bos taurus* (P16116), which shows 82% identity and 90% similarity with human ALR2, was downloaded from the Expasy homepage,⁴² and a homology model based on 2FZD, including both tolrestat and NADP⁺ as ligands, was created. Comparison with the obtained model showed that within an 8.0 Å radius of the binding site, the only sequence differences could be found at positions 297 (bovine: Ala, human: Val) and 301 (bovine: Val, human: Leu).

4. Results and discussion

4.1. Aldose reductase inhibition

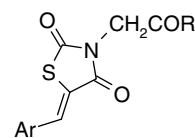
2,4-TZDs **4** and **5** were evaluated for their ability to inhibit the *in vitro* reduction of *D,L*-glyceraldehyde by partially purified ALR2 from bovine lenses; sorbinil was used as a reference drug (Table 1).

Out of acetamides **4**, [5-(4-hydroxybenzylidene)-2,4-dioxothiazolidin-3-yl]acetamide (**4i**) displayed an interesting micromolar IC₅₀ value (6.52 μM; Table 1), very close to those of the previously assayed 5-(4-hydroxybenzylidene)-2,4-thiazolidinedione and the corresponding acetic acid methyl ester (IC₅₀ = 8.96 and 6.18 μM, respectively).²⁴ In contrast, analogues **4a–g**, bearing an additional aromatic ring or a methoxy substituent in the 5-arylidene moiety, produced no or only modest ALR2 inhibition. In particular, (5-naphthalen-1-ylmethylene-2,4-dioxothiazolidin-3-yl)acetamide (**4d**) brought about 32% inhibition at 12.5 μM dose, proving to be more active than the corresponding methyl ester (12% inhibition at 50 μM dose),²⁴ whereas its 5-naphthalen-2-ylmethylene isomer **4e** was shown to be 10 times less effective at the same dose (Table 1).

The displacement of the hydroxy group of **4i** to position 3 of the 5-benzylidene ring markedly decreased inhibitory effectiveness,

Table 1

In vitro bovine lenses ALR2 inhibitory activity of 2,4-thiazolidinediones **4** and **5**



Compound	R	Ar	IC ₅₀ ^a
4a	NH ₂	3-OC ₆ H ₅ -C ₆ H ₄	8% (12.5 μM)
4b	NH ₂	4-OC ₆ H ₅ -C ₆ H ₄	n.i.
4c	NH ₂	4-C ₆ H ₅ -C ₆ H ₄	18% (12.5 μM)
4d	NH ₂	1-Naphthyl	32% (12.5 μM)
4e	NH ₂	2-Naphthyl	3% (12.5 μM)
4f	NH ₂	3-OCH ₃ -C ₆ H ₄	10% (12.5 μM)
4g	NH ₂	4-OCH ₃ -C ₆ H ₄	n.i.
4h	NH ₂	3-OH-C ₆ H ₄	16% (12.5 μM)
4i	NH ₂	4-OH-C ₆ H ₄	6.52 (4.40–9.66)
4j	NH ₂	3-OCH ₃ ,4-OH-C ₆ H ₃	31% (12.5 μM)
4k	NH ₂	3-OH,4-OCH ₃ -C ₆ H ₃	n.i.
5a	NHOH	3-OC ₆ H ₅ -C ₆ H ₄	12.7 (11.0–14.6)
5b	NHOH	4-OC ₆ H ₅ -C ₆ H ₄	3.67 (3.38–3.99)
5c	NHOH	4-OCH ₂ C ₆ H ₅ -C ₆ H ₄	7.34 (5.30–10.16)
5d	NHOH	4-C ₆ H ₅ -C ₆ H ₄	20.3 (16.5–25.0)
5e	NHOH	1-Naphthyl	4.20 (3.88–4.54)
5f	NHOH	2-Naphthyl	39% (25 μM)
5g	NHOH	4-OH-C ₆ H ₄	1.79 (1.47–2.18)
Sorbinil			1.41 (1.12–1.79)

n.i., no inhibition (0% inhibition at 12.5 μM dose).

^a IC₅₀ (μM) (95% C.L.) or% inhibition at the given concentration.

with compound **4h** producing only 16% inhibition at 12.5 μM dose. Moreover, replacing the hydrogen atom of both 3- and 4-hydroxy group of compounds **4h** and **4i** with a methyl group (compounds **4f** and **4g**) or a phenyl ring (compounds **4a** and **4b**) always led to less effective or inactive derivatives; this effect was particularly evident in the case of 4-substituted derivatives **4b** and **4g**, which were totally inefficacious (Table 1). The insertion of a methoxy group in position 3 of compound **4i** also led to a less active analogue (**4j**, 31% inhibition at 12.5 μM dose), whereas the 5-(3-hydroxy-4-methoxybenzylidene)-substituted isomer (**4k**) proved to be ineffective at 12.5 μM dose.

It may be hypothesised that the appreciable inhibitory activity of **4i** is related to the ability of the phenolic group (calculated pK_a = 9.30)³⁹ to bind the polar region of the ALR2 active site, whereas the acetamide chain might face amino acid residues of the lipophilic pocket (such as Leu300), thus making **4i** assume a 180° rotated orientation, different from the one originally expected. This hypothesis is backed up by the results from our docking studies, reported below, which indicated that the deprotonated phenol group of the 4-hydroxybenzylidene moiety of **4i** can form hydrogen bonds with Tyr48 and His110 in the catalytic centre of ALR2, whilst the acetamide chain can interact with amino acid residues of the specificity pocket of the enzyme.

The replacement of the acetamide chain on N-3 with the *N*-hydroxyacetamide one led to 2,4-TZDs **5** and provided a general significant increase in the ALR2 inhibitory effect (Table 1).

In particular, *N*-hydroxy-2-[5-(4-hydroxybenzylidene)-2,4-dioxothiazolidin-3-yl]acetamide (**5g**) exhibited an inhibitory effect (IC₅₀ = 1.79 μM) which was fourfold greater than that of analogue **4i** and very similar to that of sorbinil (Table 1).

N-Hydroxy-2-[2,4-dioxo-5-(4-phenoxybenzylidene)thiazolidin-3-yl]acetamide (**5b**) and 5-naphthalen-1-ylmethylene analogue **5e** also displayed activity in the low micromolar range (IC₅₀ = 3.67 and 4.20 μM, respectively). In contrast, the displacement of the 4-phenoxy group to position 3 of the 5-benzylidene ring (**5a**), as well as the insertion of a methylene group (**5c**), gave a two–three-

fold decrease in potency (Table 1). Analogous to what was observed for acetamides **4**, the replacement of the 5-naphthalen-1-ylmethylene moiety (**5e**) with the 5-naphthalen-2-ylmethylene one (**5f**) resulted in a significant decrease in potency.

Comparing the ALR2 inhibitory effects of *N*-hydroxyacetamides **5** with those of the corresponding acetamides **4** and carboxylic acids **3** showed an order of activity **3** > **5** > **4**. Compounds **5** were also generally more effective inhibitors (from **3** to more than 10 times) than *N*-unsubstituted analogues **1**,²⁴ probably due to the potential capability of the *N*-hydroxyacetamide chain on N-3 to interact with the biological target through a network of H bonds. However, the order of activity observed in vitro might change in vivo. In fact, the calculated p*K*_a values of *N*-hydroxyacetamides **5** ranged from 8.64 to 8.75.³⁹ Thus, at physiological pH values, compounds **5** are expected to be prevalently in non-ionized form (calculated percentage of undissociated form 95% to 96%). In contrast, carboxylic acids **3** are almost totally in their anionic form (calculated p*K*_a values in the range between 2.57 and 3.00).³⁹ The p*K*_a values of compounds **5** were also higher than those of their counterparts **1**; the latter (calculated p*K*_a = 7.60)³⁹ are expected to undergo ionisation in 38–39% percentage at physiological pH values. Therefore, derivatives **5** should be able to cross biological barriers better than previously assayed compounds **1** and **3**.

4.2. Docking results

Tables 2 and 3 summarize the results from the cross-docking of the X-ray crystal structure ligands. As can be seen from Table 2, despite the flexibility of the binding site during IFD, in four out of five cases the lowest RMSD values could be obtained when the compounds were docked into their original binding site, whilst acceptable results (RMSD ≤ 2.0) were also found in a few cases of cross-docking. In 18 out of 25 cases, the pose with the lowest InducedFitDockingScore (IFDS) value was also the one with the lowest GlideScore value (both GlideScore and IFDS have negative values, with a lower value indicating better results). In the remaining seven cases, lower RMSD was found five times by IFDS, and two times by GlideScore. In our opinion, this difference is too small to show a real advantage of using IFDS over GlideScore. In only three cases was the highest ranked pose also the one with the lowest RMSD value. These results show that whilst this method is able to find acceptable conformations close to the ligands' binding poses, both IFDS and GlideScore do not present a reliable measure

Table 3

Lowest GlideScore values obtained for cross-docking the ligands of five different X-ray crystal complexes with the IFD method

Ligand 3-letter code	Protein structure used for IFD ^a				
	1PWM	1Z3N	2FZD	2NVC	2NVD
FID	<i>-11.904</i>	-10.580	-10.709	-11.008	-9.929
3NA	<i>-11.517</i>	<i>-12.051</i>	-11.932	-12.039	-8.937
TOL	<i>-7.917</i>	<i>-9.357</i>	<i>-10.659</i>	-8.806	-6.172
ITA	<i>-11.232</i>	<i>-11.372</i>	<i>-11.527</i>	<i>-12.684</i>	-10.806
ITB	<i>-11.575</i>	<i>-11.317</i>	<i>-11.669</i>	-11.970	<i>-9.001</i>

^a Values for ligands that were docked into the protein of their original complex structure are written in italics.

to decide which conformation to choose. Interestingly, the two top-ranked poses of fidarestat showed a high RMSD of over 5.0, with the hydantoin ring wrongly placed near the backbone of Leu301 and Ser302. The same error was observed when we docked neutral fidarestat into the binding site.

As can be seen from Table 3, in four out of five cases (all complexes except 2NVD) the native ligands obtained the lowest minimum GlideScore value when docked into their original complexes. We thus believe that a low GlideScore value could be a good indicator in choosing what poses might describe the bioactive conformation of our own compounds. Interestingly, IFD of the native ligand into 2NVD also gave a ligand pose that was similar to the experimental one. No correlation with the correct poses could be observed for the IFDS, a composite score that is calculated by adding together the GlideScore value and 5% of the Prime energy from the refinement calculations.

The docking results for our six compounds are summarized in Table 4. Visual inspection of the top-ranked poses for every ligand–protein combination showed that, in contrast to the cross-docking of the crystal structure ligands, the compounds often had similar poses in different proteins. Phenols **3a**, **4i** and **5g** have their lowest GlideScore value when docked into 2NVC, followed by structurally similar 1PWM, whilst compounds **5b** and **5e** had their lowest GlideScore values when docked into 2FZD, suggesting that the hydrophobic moieties of these compounds are able to open the lipophilicity pocket. A detailed discussion of possible binding modes follows. This is based on reasonable pharmacophoric interactions, including the knowledge from the experimental data available which show that the presence of a weakly acidic group at the

Table 2

RMSD values obtained for cross-docking the ligands of five different X-ray crystal complexes with the IFD method^a

Ligand 3-letter code	Calculated RMSD	Protein structure used for IFD ^b				
		1PWM	1Z3N	2FZD	2NVC	2NVD
FID	IFDS	5.22	5.13	5.50	1.75	6.88
	GS	5.22	5.13	5.50	1.75	6.88
	Minimum	<i>0.67</i>	4.42	2.66	1.44	5.45
3NA	IFDS	1.51	<i>0.70</i>	2.00	3.12	5.49
	GS	1.31	<i>0.70</i>	2.00	3.12	7.11
	Minimum	1.04	<i>0.67</i>	1.94	2.37	3.56
TOL	IFDS	1.48	1.20	1.79	4.18	5.52
	GS	1.48	1.20	3.23	4.70	5.52
	Minimum	1.48	<i>0.78</i>	1.76	1.65	3.47
ITA	IFDS	1.46	4.80	7.16	<i>0.88</i>	6.83
	GS	7.19	4.80	7.16	<i>0.88</i>	6.80
	Minimum	0.98	4.37	1.76	0.75	5.56
ITB	IFDS	1.41	5.48	4.08	7.79	1.65
	GS	1.41	5.34	4.08	7.79	1.65
	Minimum	1.41	4.49	4.08	1.22	1.12

^a RMSD values are shown for the pose with lowest InducedFitDockingScore (IFDS), lowest GlideScore (GS) and minimum RMSD value amongst all poses (minimum).

^b Values for ligands that were docked into the protein of their original complex structure are written in italics.

Table 4

Lowest GlideScore values obtained for induced-fit docking of six selected compounds into five different protein conformations from X-ray crystal complexes^a

Compound	Protein structure used for IFD				
	1PWM	1Z3N	2FZD	2NVC	2NVD
3a	<i>-12.156</i>	<i>-11.394</i>	<i>-11.312</i>	<i>-12.934</i>	<i>-11.365</i>
4g	<i>-8.739</i>	<i>-8.943</i>	<i>-9.433</i>	<i>-9.473</i>	<i>-7.356</i>
4i	<i>-11.751</i>	<i>-10.643</i>	<i>-11.285</i>	<i>-12.416</i>	<i>-10.066</i>
5b	<i>-7.966</i>	<i>-8.901</i>	<i>-11.472</i>	<i>-8.575</i>	<i>-9.521</i>
5e	<i>-7.423</i>	<i>-10.701</i>	<i>-11.572</i>	<i>-10.259</i>	<i>-8.472</i>
5g	<i>-11.687</i>	<i>-10.992</i>	<i>-11.065</i>	<i>-11.926</i>	<i>-10.362</i>

^a For each ligand, the lowest GlideScore values are written in italics.

catalytic centre is an important factor. Possible binding modes are also based on a low GlideScore value, but within the limits stated above.

The inspection of the highest ranked docking poses gave similar results for 5-(4-hydroxybenzylidene) derivatives **3a**, **4i** and **5g** (exemplified by **3a**, Fig. 4 left side). All of these compounds appear to bind in a mode that is flipped in comparison to the one originally proposed. In particular, for compound **3a**, we received a pose that is quite different from the one that we had suggested previously.²⁴ Thus, the deprotonated phenol group incorporates the catalytic centre with the usual hydrogen bonds donated by Tyr48 and His110, whilst the acetic acid side chain forms a tight net of hydrogen bonds with the surrounding backbone NH groups of Leu301 and Ser302 as well as the hydroxyl group of Ser302. In addition, the carbonyl group at position 2 of the thiazolidinedione ring forms a hydrogen bond with the backbone NH groups of Leu300 and Ala299. Finally, a weak hydrogen bond between the thiol group of Cys298 and the ring sulfur atom of the ligands is suggested. The carboxylic acid **3a**, which showed the highest activity amongst the three compounds, is also able to establish the highest number of hydrogen bonds by interacting with every backbone NH group from Ala299 to Ser302 and also with the hydroxyl group of Ser302. It should be noted that similar interactions with Ser302 can be seen in 2NVC, where the acetic acid side chain of the ligand that is connected via the ester group is placed at a similar position (Fig. 3). Although no positive charge is located in close vicinity of the backbone binding area between Ala299 and Ser302, the multiple donated hydrogen bonds should be well able to stabilize the negative charge of the carboxylates. These results also provide a possible explanation as to why the phenol derivative **4i** is the only compound from the amide series which shows such a high affinity, whilst other amides that have a highly active twin in the *N*-hydroxyacetamide series (**4b/5b**; **4d/5e**) or in the acetic acid series^{23–25} (**4a–d**, **4f**, **4h**, **4j**, and **4k**) are virtually inactive or barely active. Furthermore, if compounds of series **4** were to bind to the catalytic centre via the amide group, then small alterations at the phenyl ring as seen for compounds **4f**, **4g**, **4h**, **4j** and **4k** should not have such a big impact on the binding, since these groups would then point outwards from the binding site. A similar correlation is also seen in our acetic acid methyl ester series reported earlier, where the corresponding compound (Ar = 4-OH-C₆H₄, IC₅₀ = 6.18 M)²⁴ is one of the few derivatives with micromolar affinity.

The second investigated acetamide derivative **4g**, which was inactive in our assays, gave the highest GlideScore values (Table 4) with its lowest score lying at 1.999 or more above the lowest score for the other investigated compounds.

For the more lipophilic compounds **5b** and **5e**, 5-(4-phenoxybenzylidene)- and 5-naphthalen-1-ylmethylidene substituted, respectively, we received a second type of pose that suggests interactions with the lipophilic selectivity pocket in a way similar to that of tolrestat (exemplified by **5b**, Fig. 4 right side). In these

poses, the phenoxyphenyl residue of **5b** has lipophilic contacts with the surrounding side chain residues of Phe115, Phe122, Leu124 and Leu300, whilst the 1-naphthyl group of **5e** is surrounded by the side chain residues of Phe115, Phe122, Val130 and Leu300. Furthermore, when docking **5e** into 1Z3N, we found a pose similar to that of lidorestat, with the naphthyl residue forming π - π interactions with Trp111, and additional lipophilic contacts with Phe115, Phe122 and Leu300.

The program LigandScout v2.0,⁴³ which allows 3D pharmacophores from macromolecule/ligand complexes to be rapidly derived in a fully automated way, was used to visualize the pharmacophoric interactions of **3a** and **5b**, respectively, with the binding site in both 3D and 2D depiction (Fig. 4, middle and bottom row). The detected interactions fit well with our observations discussed above.

As seen from both the cross-docking results and the poses received from docking our own compounds, there were no big structural changes within the overall structure of the chosen binding pocket conformations with the settings we selected (temporarily mutating only the side chain of Leu300 to Ala, scaling of the van der Waals radii for the receptor atoms by 70%). One might thus wonder whether it is reasonable at all to use an induced-fit docking method in this case, or whether an ensemble docking approach, using a number of different rigid binding sites, would also have been successful. In an attempt to answer this question, we docked **5b** into the rigid binding pocket of 2FZD, using Glide with default settings and no constraints. The best-ranked pose obtained from this experiment showed a GlideScore value of -6.76, in contrast to -11.472 obtained in the IFD experiment where the same binding pocket was used. Additionally, no interactions with the catalytic centre were found by any pose from this run. Since the best pose obtained during the IFD run of **5b** into 2FZD was not retrieved in any other IFD experiment, we would have simply missed this reasonable pose when using only rigid binding pockets.

Regarding the validity of using structural information of human vs. bovine aldose reductase, we came to the following conclusion: whilst both Leu300 and Ser302 play an important role in the binding of the ligands, the side chain of Leu resp. Val301 points away from the binding site. We obtained no results from the docking into the human structures that would suggest an important role of this residue in ligand binding. The side chain of the protein at position 297 is even further away from both experimental and modeled ligand poses. Moreover, compounds docked into the homology model gave results similar to those of docking into 2FZD. We thus conclude that comparing binding and modeling studies between bovine and human ALR2 proteins is a valid approach.

5. Conclusion

The in vitro evaluation of (5-arylidene-2,4-dioxothiazolidin-3-yl)acetamides (**4**) and analogous *N*-hydroxyacetamides (**5**) highlighted that the replacement of the carboxylic anionic head of acids **3** with the carboxamide or *N*-hydroxycarboxamide group produces a general decrease in the in vitro ALR2 inhibitory effect, whereas in comparison with *N*-unsubstituted analogues **1**, the insertion of the *N*-hydroxyacetamide chain on N-3 (compounds **5**) gave a general improvement in activity.

Our docking studies suggest that the appreciable inhibitory activity of **4i**, which stands out amongst compounds **4**, is related to the capability of the phenolic group to bind the polar region of the ALR2 active site.

Out of our novel non-carboxylic acid bearing 2,4-thiazolidinedione derivatives **4** and **5** the ones that exhibited micromolar ALR2 binding affinity will be used as starting points for a future drug discovery programme aimed at enhancing their activity profiles and evaluating their in vivo effectiveness.

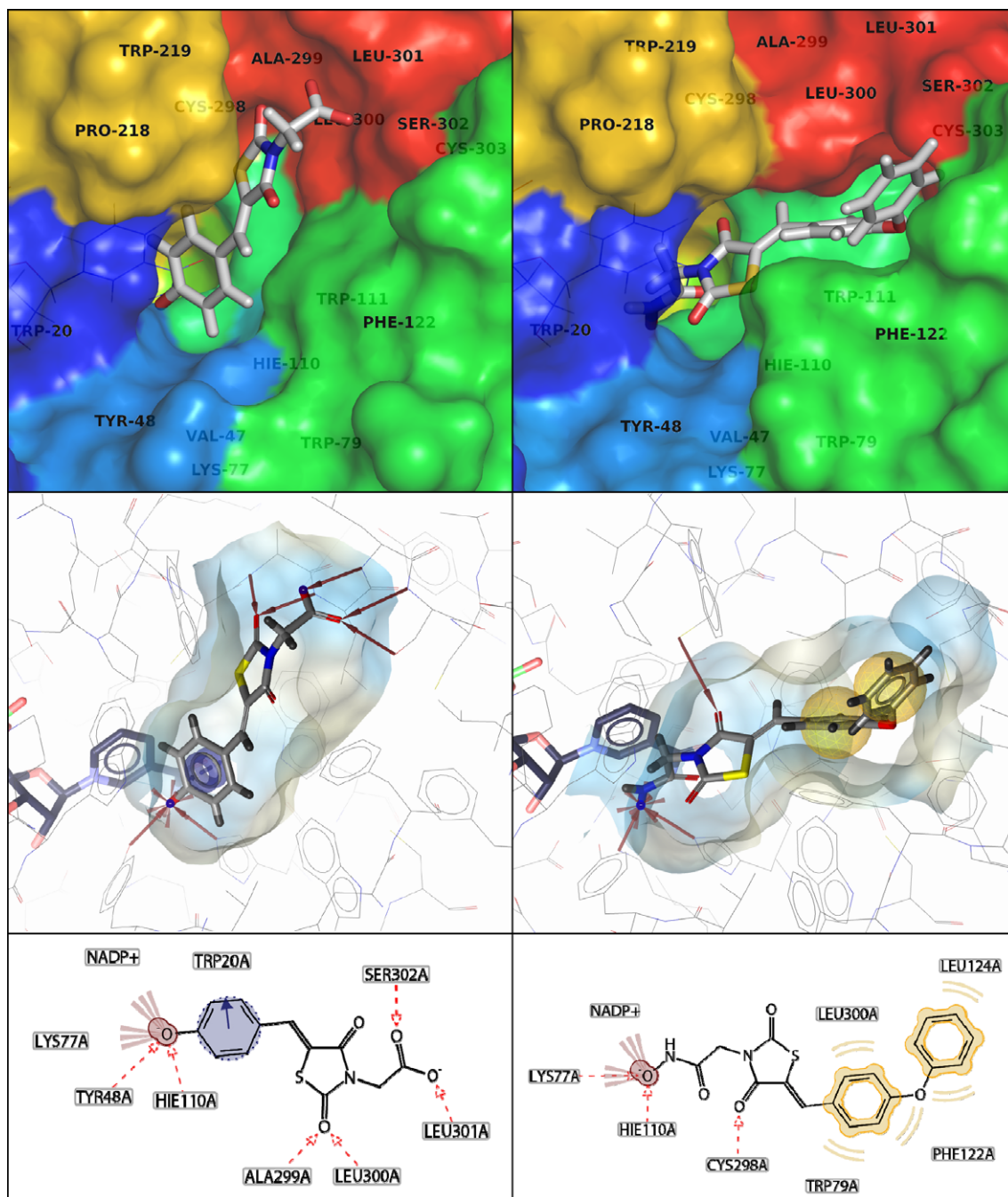


Figure 4. Depiction of the two major types of binding modes predicted for our ligands, based on the lowest GlideScore values in Table 4, exemplified by **3a** docked into 2NVC (left side),³⁷ and **5b** docked into 2FZD (right side).³⁵ Top: Docked poses displayed in PyMOL,⁴⁶ same representation as in Figure 3. Middle: The same poses visualized in LigandScout,⁴³ with pharmacophore features detected by the software. Features showing pharmacophoric interactions between ligand and binding site: red arrows: hydrogen bond acceptors, red star: negative ionizable/charged, purple ring and arrows: aromatic plane, yellow spheres: hydrophobic. The cofactor NADP⁺, placed behind the ligands in this view, is represented in stick-mode. Bottom: 2D depiction of interactions detected by LigandScout with the surrounding amino acids and the cofactor. HIE: histidine (HIS) with hydrogen on the epsilon nitrogen, as assigned by Maestro during the protein preparation step.

We have elaborated a procedure for induced-fit docking of compounds into the binding pocket of ALR2, taking into account the diverse complex structures available as well as the current knowledge regarding the protonation state of the ligands. The promising results give us a possible explanation of our binding data, especially for the 5-(4-hydroxybenzylidene) derivatives from our different series. Our IFD studies indicate that these latter can bind to the catalytic centre via the deprotonated phenol group and that they can form a number of hydrogen bonds with the protein backbone near Ser 302 via the acetic chain. A bind-

ing mode that is closer to the previously assumed one,²⁴ where the carboxylic or hydroxamic acid residue is located at the recognition region and the arylidene residue is placed at the hydrophobic specificity pocket of the enzyme, is suggested for compounds with a more lipophilic and non-acidic arylidene residue. We think that the working procedure presented herein has expanded the knowledge about the applicability of induced-fit docking methodology. It has also aided the modelling of this well-known target protein which, due to the flexibility of its binding site, is still highly challenging.

6. Experimental

6.1. Chemistry

Melting points were recorded on a Kofler hot-stage apparatus and are uncorrected. TLC controls were carried out on pre-coated silica gel plates (F 254 Merck). Elemental analyses (C, H, N), determined by means of a C. Erba mod. 1106 elem. Analyzer, were within $\pm 0.4\%$ of theory. ^1H and ^{13}C NMR spectra were recorded on a Varian 300 magnetic resonance spectrometer (300 MHz for ^1H and 75 MHz for ^{13}C). Chemical shifts are given in δ units (ppm) relative to internal standard Me_4Si and refer to $\text{DMSO}-d_6$ solutions. Coupling constants (J) are given in hertz (Hz). ^{13}C NMR spectra were determined by Attached Proton Test (APT) experiments and the resonances were always attributed by proton-carbon heteronuclear chemical shift correlation. A microwave oven Discover (CEM) was used to carry out microwave-assisted reactions. Unless stated otherwise, all materials were obtained from commercial suppliers and used without further purification.

6.2. General method for the synthesis of 2-(5-arylidene-2,4-dioxothiazolidin-3-yl)acetamides (4a–k)

A mixture of 5-arylidene-2,4-thiazolidinedione **1** (17 mmol) and potassium carbonate (1.93 g, 14 mmol) in acetonitrile was refluxed for 45 min. Then a solution of 2-chloroacetamide (1.87 g, 20 mmol) in acetonitrile was slowly added and the mixture was refluxed for 24–72 h. After evaporation of the solvent under reduced pressure, the crude solid was washed with water, until the pH value of the filtrate was neutral, and then with acetonitrile, to give pure acetamide **4**.

Compounds **4h–k** were synthesised as described above, adding a solution of 2-chloroacetamide (1.59 g, 17 mmol) in acetonitrile dropwise to a solution of compound **1** (17 mmol) and potassium carbonate (1.93 g, 14 mmol) in acetonitrile for 2 h.

6.2.1. (Z)-2-[2,4-Dioxo-5-(3-phenoxybenzylidene)thiazolidin-3-yl]acetamide (4a)

Yield 64%; mp 238–239 °C; ^1H NMR ($\text{DMSO}-d_6$): δ 4.19 (s, 2H, NCH_2); 7.06–7.57 (3m, 9H, arom); 7.33 and 7.76 (2 br s exchangeable with D_2O , 2H, NH_2); 7.94 (s, 1H, CH). ^{13}C NMR ($\text{DMSO}-d_6$): δ 43.8 (NCH_2); 119.4, 119.7, 120.8, 124.6, 125.2, 130.7, 131.5 (CH arom); 122.6 (5-C); 133.0 (CH methylidene); 135.2, 156.2, 158.0 (Cq arom); 165.5, 167.1, 167.3 (C=O); Anal. ($\text{C}_{18}\text{H}_{14}\text{N}_2\text{O}_4\text{S}$) C, H, N.

6.2.2. (Z)-2-[2,4-Dioxo-5-(4-phenoxybenzylidene)thiazolidin-3-yl]acetamide (4b)

Yield 49%; mp 198–200 °C; ^1H NMR ($\text{DMSO}-d_6$): δ 4.19 (s, 2H, NCH_2); 7.07–7.23 (2m, 5H, arom); 7.30 and 7.71 (2 br s exchangeable with D_2O , 2H, NH_2); 7.40–7.45 (m, 2H, arom); 7.65 (m, 2H, arom); 7.90 (s, 1H, CH); ^{13}C NMR ($\text{DMSO}-d_6$): δ 43.7 (NCH_2); 118.8, 120.3, 125.1, 130.7, 132.9 (CH arom); 120.0 (5-C); 133.1 (CH methylidene); 128.0, 155.6, 159.7 (Cq arom); 165.8, 167.3, 167.5 (C=O); Anal. ($\text{C}_{18}\text{H}_{14}\text{N}_2\text{O}_4\text{S}$) C, H, N.

6.2.3. (Z)-2-(5-Biphenyl-4-ylmethylene-2,4-dioxothiazolidin-3-yl)acetamide (4c)

Yield 24%; mp 244–245 °C; ^1H NMR ($\text{DMSO}-d_6$): δ 4.24 (s, 2H, NCH_2); 7.33 and 7.69 (2 br s exchangeable with D_2O , 2H, NH_2); 7.41–7.54 (2m, 3H, arom); 7.73–7.77 (m, 4H, arom); 7.87 (m, 2H, arom); 8.01 (s, 1H, CH); ^{13}C NMR ($\text{DMSO}-d_6$): δ 44.0 (NCH_2); 121.7 (5-C); 127.5, 128.2, 129.2, 129.9, 131.6 (CH arom); 133.6 (CH methylidene); 132.6, 139.4, 142.9 (Cq arom); 166.2, 167.9, 168.0 (C=O); Anal. ($\text{C}_{18}\text{H}_{14}\text{N}_2\text{O}_3\text{S}$) C, H, N.

6.2.4. (Z)-2-(5-Naphthalen-1-ylmethylene-2,4-dioxothiazolidin-3-yl)acetamide (4d)

Yield 77%; mp 296–298 °C; ^1H NMR ($\text{DMSO}-d_6$): δ 4.27 (s, 2H, NCH_2); 7.35 and 7.58 (2 br s exchangeable with D_2O , 2H, NH_2); 7.64–8.14 (2m, 7H, arom); 8.58 (s, 1H, CH); ^{13}C NMR ($\text{DMSO}-d_6$): δ 43.8 (NCH_2); 123.9, 126.2, 127.1, 127.5, 128.1, 129.5, 130.9 (CH arom); 125.4 (5-C); 131.6 (CH methylidene); 130.7, 131.5, 133.8 (Cq arom); 165.4, 167.5, 168.0 (C=O); Anal. ($\text{C}_{16}\text{H}_{12}\text{N}_2\text{O}_3\text{S}$) C, H, N.

6.2.5. (Z)-2-(5-Naphthalen-2-ylmethylene-2,4-dioxothiazolidin-3-yl)acetamide (4e)

Yield 22%; mp 266–269 °C; ^1H NMR ($\text{DMSO}-d_6$): δ 4.26 (s, 2H, NCH_2); 7.35 and 7.77 (2 br s exchangeable with D_2O , 2H, NH_2); 7.61–8.10 (3m, 7H, arom); 8.25 (s, 1H, CH); ^{13}C NMR ($\text{DMSO}-d_6$): δ 43.8 (NCH_2); 122.0 (5-C); 126.4, 127.7, 128.2, 128.6, 129.3, 129.5, 131.6 (CH arom); 131.0, 133.2, 133.9 (Cq arom); 133.7 (CH methylidene); 165.8, 167.3, 167.6 (C=O); Anal. ($\text{C}_{16}\text{H}_{12}\text{N}_2\text{O}_3\text{S}$) C, H, N.

6.2.6. (Z)-2-[5-(3-Methoxybenzylidene)-2,4-dioxothiazolidin-3-yl]acetamide (4f)

Yield 63%; mp 210–212 °C; ^1H NMR ($\text{DMSO}-d_6$): δ 3.81 (s, 3H, OCH_3); 4.23 (s, 2H, NCH_2); 7.12 (d, $J = 8.9$ Hz, 1H, arom); 7.22 (m, 2H, arom); 7.50 (dd $J = 8.9$ and 8.9 Hz, 1H, arom); 7.34 and 7.75 (2 br s exchangeable with D_2O , 2H, NH_2); 7.93 (s, 1H, CH); ^{13}C NMR ($\text{DMSO}-d_6$): δ 43.3 (NCH_2); 55.3 (OCH_3); 115.5, 116.6, 121.9, 130.5 (CH arom); 121.5 (5-C); 133.2 (CH methylidene); 134.2, 159.6 (Cq arom); 165.3, 166.8, 167.1 (C=O); Anal. ($\text{C}_{13}\text{H}_{12}\text{N}_2\text{O}_4\text{S}$) C, H, N.

6.2.7. (Z)-2-[5-(4-Methoxybenzylidene)-2,4-dioxothiazolidin-3-yl]acetamide (4g)

Yield 32%; mp 263–264 °C; ^1H NMR ($\text{DMSO}-d_6$): δ 3.84 (s, 3H, OCH_3); 4.23 (s, 2H, NCH_2); 7.13 (m, 2H, arom); 7.61 (m, 2H, arom); 7.34 and 7.74 (2 br s exchangeable with D_2O , 2H, NH_2); 7.92 (s, 1H, CH); ^{13}C NMR ($\text{DMSO}-d_6$): δ 43.8 (NCH_2); 56.2 (OCH_3); 115.6, 132.7 (CH arom); 125.9 (5-C); 133.8 (CH methylidene); 118.5, 161.7 (Cq arom); 165.9, 167.3, 167.6 (C=O); Anal. ($\text{C}_{13}\text{H}_{12}\text{N}_2\text{O}_4\text{S}$) C, H, N.

6.2.8. (Z)-2-[5-(3-Hydroxybenzylidene)-2,4-dioxothiazolidin-3-yl]acetamide (4h)

Yield 49%; mp 251–253 °C; ^1H NMR ($\text{DMSO}-d_6$): δ 4.22 (s, 2H, NCH_2); 6.90 (dd, $J = 7.8$ and 1.5 Hz, 1H, arom); 7.01 (s, 1H, arom); 7.08 (d, $J = 7.8$ Hz, 1H, arom); 7.34 (dd, $J = 7.8$ and 7.8 Hz, 1H, arom); 7.31 and 7.74 (2 br s exchangeable with D_2O , 2H, NH_2); 7.86 (s, 1H, CH); 9.90 (br s exchangeable with D_2O , 1H, OH); ^{13}C NMR ($\text{DMSO}-d_6$): δ 43.8 (NCH_2); 116.6, 118.6, 122.0, 131.1 (CH arom); 121.7 (5-C); 134.0 (CH methylidene); 134.7, 158.5 (Cq arom); 165.8, 167.3, 167.6 (C=O); Anal. ($\text{C}_{12}\text{H}_{10}\text{N}_2\text{O}_4\text{S}$) C, H, N.

6.2.9. (Z)-2-[5-(4-Hydroxybenzylidene)-2,4-dioxothiazolidin-3-yl]acetamide (4i)

Yield 37%; mp 268–270 °C; ^1H NMR ($\text{DMSO}-d_6$): δ 4.19 (s, 2H, NCH_2); 6.90 (m, 2H, arom); 7.48 (m, 2H, arom); 7.29 and 7.69 (2 br s exchangeable with D_2O , 2H, NH_2); 7.82 (s, 1H, CH); 10.35 (br s exchangeable with D_2O , 1H, OH); ^{13}C NMR ($\text{DMSO}-d_6$): δ 43.8 (NCH_2); 117.0, 133.1 (CH arom); 117.2 (5-C); 134.2 (CH methylidene); 124.4, 160.8 (Cq arom); 166.0, 167.4, 167.7 (C=O); Anal. ($\text{C}_{12}\text{H}_{10}\text{N}_2\text{O}_4\text{S}$) C, H, N.

6.2.10. (Z)-2-[5-(4-Hydroxy-3-methoxybenzylidene)-2,4-dioxothiazolidin-3-yl]acetamide (4j)

Yield 42%; mp 243–245 °C; ^1H NMR ($\text{DMSO}-d_6$): δ 3.82 (s, 3H, OCH_3); 4.20 (s, 2H, NCH_2); 6.93 (d, $J = 8.7$ Hz, 1H, arom); 7.11 (d, $J = 8.7$ Hz, 1H, arom); 7.21 (s, 1H, arom); 7.30 and 7.71 (2 br s exchangeable with D_2O , 2H, NH_2); 7.84 (s, 1H, CH); 10.02 (br s

exchangeable with D₂O, 1H, OH); ¹³C NMR (DMSO-*d*₆): δ 43.7 (NCH₂); 56.1 (OCH₃); 114.8, 116.7, 124.9 (CH arom); 117.5 (5-C); 134.3 (CH methylidene); 125.0, 148.6, 150.3 (Cq arom); 165.8, 167.3, 167.9 (C=O); Anal. (C₁₃H₁₂N₂O₅S) C, H, N.

6.2.11. (Z)-2-[5-(3-Hydroxy-4-methoxybenzylidene)-2,4-dioxothiazolidin-3-yl]acetamide (4k)

Yield 60%; mp 268–270 °C; ¹H NMR (DMSO-*d*₆): δ 3.81 (s, 3H, OCH₃); 4.20 (s, 2H, NCH₂); 7.06–7.15 (m, 3H, arom); 7.31 and 7.71 (2 br s exchangeable with D₂O, 2H, NH₂); 7.79 (s, 1H, CH); 9.54 (br s exchangeable with D₂O, 1H, OH); ¹³C NMR (DMSO-*d*₆): δ 43.7 (NCH₂); 56.2 (OCH₃); 113.1, 116.5, 124.2 (CH arom); 118.2 (5-C); 134.2 (CH methylidene); 126.1, 147.5, 151.0 (Cq arom); 166.0, 167.4, 167.8 (C=O); Anal. (C₁₃H₁₂N₂O₅S) C, H, N.

6.3. General method for the synthesis of 2-(5-arylidene-2,4-dioxothiazolidin-3-yl)-N-hydroxyacetamides (5a–g)

Method (A): A mixture of (5-arylidene-2,4-dioxothiazolidin-3-yl)acetic acid **3** (14 mmol), ethyl chlorofomate (2.38 g, 22 mmol) and triethylamine (2.55 g, 25.2 mmol) in diethylether was stirred at 0 °C for 15 min. At the same time, a solution of hydroxylamine hydrochloride (1.45 g, 21 mmol) in anhydrous methanol was added to a solution of sodium hydroxide (0.84 g, 21 mmol) in anhydrous methanol; the mixture was stirred at 0 °C for 15 min; then the solid was removed and the filtrate was used as such. The former mixture was added to this freshly prepared solution of hydroxylamine and stirred at room temperature for 24–40 h. After evaporation of the solvent in vacuo, the crude solid was washed with diethylether; the solid was dried and then washed with water to provide pure compound **5**.

Method (B): A mixture of (5-arylidene-2,4-dioxothiazolidin-3-yl)acetic acid **3** (14 mmol), ethyl chlorofomate (2.38 g, 22 mmol) and triethylamine (2.55 g, 25.2 mmol) in diethylether in a hermetically sealed vial was irradiated with microwaves (80 °C, max 150 psi, max 300 W) for 5 min. At the same time, a solution of hydroxylamine hydrochloride (1.45 g, 21 mmol) in anhydrous methanol was added to a solution of sodium hydroxide (0.84 g, 21 mmol) in anhydrous methanol; the mixture was stirred at 0 °C for 15 min; then the solid was removed and the filtrate was used as such. The former mixture was added to the freshly prepared solution of hydroxylamine and the mixture was irradiated with microwaves (80 °C, max 150 psi, max 300 W) for 5 min. After evaporation of the solvent in vacuo, the crude solid was washed with diethylether; the solid was dried and then washed with water to provide pure compound **5**. Yields reported below refer to *method B*.

6.3.1. (Z)-N-Hydroxy-2-[2,4-Dioxo-5-(3-phenoxybenzylidene)-thiazolidin-3-yl]acetamide (5a)

Yield 45%; mp > 230 °C ¹H NMR (DMSO-*d*₆): δ 4.19 (s, 2H, NCH₂); 7.09–7.59 (3m, 9H, arom); 7.95 (s, 1H, CH); 9.03 and 10.86 (2 br s exchangeable with D₂O, 2H, NH and OH); ¹³C NMR (DMSO-*d*₆): δ 42.0 (NCH₂); 119.4, 119.7, 120.8, 124.6, 125.2, 130.7, 131.5 (CH arom); 122.5 (5-C); 133.2 (CH methylidene); 135.2, 156.2, 158.1 (Cq arom); 162.6, 167.3, 168.0 (C=O); Anal. (C₁₈H₁₄N₂O₅S) C, H, N.

6.3.2. (Z)-N-hydroxy-2-[2,4-Dioxo-5-(4-phenoxybenzylidene)-thiazolidin-3-yl]acetamide (5b)

Yield 60%; mp 170 °C; ¹H NMR (DMSO-*d*₆): δ 4.19 (s, 2H, NCH₂); 7.09–7.11 (m, 4H, arom); 7.21 (m, 1H, arom); 7.43 (m, 2H, arom); 7.66 (m, 2H, arom); 7.93 (s, 1H, CH); 9.04 and 10.85 (2 br s exchangeable with D₂O, 2H, NH and OH); ¹³C NMR (DMSO-*d*₆): δ 42.0 (NCH₂); 119.9 (5-C); 118.8, 120.4, 125.2, 130.8, 133.0 (CH

arom); 133.3 (CH methylidene); 128.1, 155.6, 159.7 (Cq arom); 162.8, 167.5, 168.2 (C=O); Anal. (C₁₈H₁₄N₂O₅S) C, H, N.

6.3.3. (Z)-2-[5-(4-Benzyloxybenzylidene)-2,4-dioxothiazolidin-3-yl]-N-hydroxyacetamide (5c)

Yield 65%; mp 164–165 °C; ¹H NMR (DMSO-*d*₆): δ 4.63 (s, 2H, NCH₂); 5.20 (s, 2H, OCH₂); 7.20 (m, 2H, arom); 7.37–7.47 (m, 5H, arom); 7.62 (m, 2H, arom); 7.97 (s, 1H, CH); 9.02 and 10.82 (2 br s exchangeable with D₂O, 2H, NH and OH); ¹³C NMR (DMSO-*d*₆): δ 46.2 (NCH₂); 70.3 (OCH₂); 118.0 (5-C); 116.6, 128.2, 128.5, 129.3, 133.2 (CH arom); 134.9 (CH methylidene); 126.1, 137.2, 160.5 (Cq arom); 163.7, 166.3, 167.6 (C=O); Anal. (C₁₉H₁₆N₂O₅S) C, H, N.

6.3.4. (Z)-2-(5-Biphenyl-4-ylmethylene-2,4-dioxothiazolidin-3-yl)-N-hydroxyacetamide (5d)

Yield 40%; mp 219–220 °C; ¹H NMR (DMSO-*d*₆): δ 4.21 (s, 2H, NCH₂); 7.40–7.52 (m, 4H, arom); 7.72–7.76 (m, 3H, arom); 7.83 (m, 2H, arom); 7.98 (s, 1H, CH); 9.05 and 10.98 (2 br s exchangeable with D₂O, 2H, NH and OH); ¹³C NMR (DMSO-*d*₆): δ 41.5 (NCH₂); 120.7 (5-C); 126.8, 127.5, 128.2, 129.1, 130.8 (CH arom); 132.8 (CH methylidene); 132.0, 138.6, 142.0 (Cq arom); 163.5, 166.7, 167.6 (C=O); Anal. (C₁₈H₁₄N₂O₄S) C, H, N.

6.3.5. (Z)-N-Hydroxy-2-(5-Naphthalen-1-ylmethylene-2,4-dioxothiazolidin-3-yl)acetamide (5e)

Yield 53%; mp 218–219 °C; ¹H NMR (DMSO-*d*₆): δ 4.24 (s, 2H, NCH₂); 7.61–7.73 (m, 3H, arom); 8.02–8.11 (m, 4H, arom); 8.58 (s, 1H, CH); 9.07 and 10.99 (2 br s exchangeable with D₂O, 2H, NH and OH); ¹³C NMR (DMSO-*d*₆): δ 42.2 (NCH₂); 125.3 (5-C); 123.9, 126.1, 126.9, 127.4, 128.1, 129.4, 130.8 (CH arom); 131.5 (CH methylidene); 130.6, 131.4, 133.8 (Cq arom); 162.7, 167.8, 168.1 (C=O); Anal. (C₁₆H₁₂N₂O₄S) C, H, N.

6.3.6. (Z)-N-Hydroxy-2-(5-Naphthalen-2-ylmethylene-2,4-dioxothiazolidin-3-yl)acetamide (5f)

Yield 46%; mp 286–287 °C dec.; ¹H NMR (DMSO-*d*₆): δ 4.24 (s, 2H, NCH₂); 7.58–7.70 (m, 3H, arom); 7.93–8.10 (m, 4H, arom); 8.18 (s, 1H, CH); 9.06 and 11.00 (2 br s exchangeable with D₂O, 2H, NH and OH); ¹³C NMR (DMSO-*d*₆): δ 42.0 (NCH₂); 124.4 (5-C); 126.5, 127.6, 128.2, 128.5, 129.2, 129.4, 131.3 (CH arom); 132.2 (CH methylidene); 131.2, 133.2, 133.8 (Cq arom); 162.5, 167.9, 168.4 (C=O); Anal. (C₁₆H₁₂N₂O₄S) C, H, N.

6.3.7. (Z)-N-Hydroxy-2-[5-(4-Hydroxybenzylidene)-2,4-dioxothiazolidin-3-yl]acetamide (5g)

Yield 63%; mp 155–157 °C. ¹H NMR (DMSO-*d*₆): δ 4.19 (s, 2H, NCH₂); 6.96 (m, 2H, arom); 7.53 (m, 2H, arom); 7.88 (s, 1H, CH); 8.63, 9.01 and 10.82 (3 br s exchangeable with D₂O, 3H, NH and 2 OH). ¹³C NMR (DMSO-*d*₆): δ 43.9 (NCH₂); 117.0, 133.1 (CH arom); 124.3 (5-C); 134.2 (CH methylidene); 124.8, 160.8 (Cq arom); 166.0, 167.7, 168.6 (C=O); Anal. (C₁₂H₁₀N₂O₅S) C, H, N.

6.4. Molecular modeling

All molecular modeling studies were performed using the Schrodinger Suite 2007, including Maestro 8.0, Glide 4.5, and Prime 1.6,⁴¹ on a PC equipped with a 2.13 GHz Core 2 Duo processor and 1 GB of RAM, running Fedora Core 6 Linux.

The IFD protocol developed by Schrödinger, LLC⁴⁰ consists of three main steps, that may be summarized as follows. First, an initial docking run is performed with the Glide docking module, during which the van der Waals radii of both ligand and binding site atoms are scaled (by 50% for both, if no side chains are selected for removal, otherwise by 50% for the ligand and 70% for the receptor), and user-selected side chains are temporarily mutated

to alanine, to reduce steric clashes. In the second step, the replaced residues are restored and side-chain prediction and minimization are performed with the Prime module for a given number of structures (20 by default) of every ligand–protein complex obtained in the first step. In the final step, the ligands are redocked into the induced-fit structures from the previous stage that fall within a given energy value of the lowest energy structure (default value 30 kcal/mol).

The selected PDB structures were processed in Maestro (Schrödinger, LLC)⁴¹ using the Protein Preparation Wizard, which performs the following steps: assigning of bond orders, addition of hydrogens, optimization of hydrogen bonds by flipping amino side chains, correction of charges, and minimization of the protein complex. All water molecules were removed from the protein structure. Automatically assigned bond orders, protonation states of the ligands, and the orientation and tautomeric state of His110 were inspected manually and corrected where necessary. For easy comparison of the results produced by docking into the different complexes, the five selected complexes were aligned with the Protein Structure Alignment tool in Maestro.

All acidic groups, including the weaker phenolic and hydroxamic acids and the hydantoin residue of fidarestat, were prepared in their deprotonated state. All ligands that were selected for docking were minimized using the OPLS_2005 force field.

The selected ligands were then docked into each of the five prepared protein binding sites, using the Induced-Fit Docking workflow accessible via the Maestro graphical interface. The pocket was defined by selecting the ligand that is part of the respective complex. In order to take into account the high flexibility of Leu300, the side chain of this residue was changed to Ala in the initial docking step. The other settings were used at their default values, with Protein Prep constrained refinement turned on, van der Waals radius scaling of 0.7 for the protein and 0.5 for the ligand, standard precision to be used during both initial docking and final redocking, a maximum of 20 poses to be carried forward for each ligand after initial docking, refining of residues within 5.0 Å of the ligand poses, optimization of the side chains, and redocking into structures within 30.0 kcal/mol of the best and within the top 20 overall structures.

Comparison of the cross-docking poses was performed by RMSD calculation on the redocked native ligands and their corresponding experimentally obtained conformations using the Superposition tool, after import of the previously aligned protein structures and without transformation of coordinates during superposition.

6.5. Determination of the in vitro aldose reductase inhibition

NADPH, D,L-glyceraldehyde and dithiothreitol (DTT) were purchased from Sigma Chemical Co. DEAE-cellulose (DE-52) was obtained from Whatman. Sorbinil was a gift from Prof. Dr. Luca Costantino, University of Modena (Italy) and was used as standard. All other chemicals were commercial samples of good grade. Calf lenses for the isolation of ALR2 were obtained locally from freshly slaughtered animals. The enzyme was isolated and purified by a chromatographic procedure as previously described.⁴⁴ Briefly, ALR2 was released by carving the capsule and the frozen lenses were suspended in potassium phosphate buffer pH 7.0 containing 5 mM DTT and stirred in an ice-cold bath for two hours. The suspension was centrifuged for 30 min at 4000 rpm at 4 °C and the supernatant was subjected to ion exchange chromatography on DE-52. Enzyme activity was assayed spectrophotometrically on a Cecil Super Auris CE 3041 spectrophotometer by measuring the decrease in absorption of the cofactor NADPH at 340 nm which accompanies the oxidation of NADPH catalyzed by the enzyme. The assay was performed at 37 °C in a reaction mixture containing

0.25 M potassium phosphate buffer pH 6.8, 0.38 M ammonium sulfate, 0.11 mM NADPH and 4.7 mM D,L-glyceraldehyde as substrate in a final volume of 1.5 mL. All inhibitors were dissolved in DMSO, the final concentration of this solvent in the reaction mixture was 1%. To correct for the non-enzymatic oxidation of the cofactor, the rate of NADPH oxidation in the presence of all the components except the substrate was subtracted from each experimental rate. Each dose–effect curve was generated using at least three concentrations of inhibitor that caused an inhibition between 20% and 80%. Each concentration was tested in duplicate and IC₅₀ values as well as the 95% confidence limits (95% CL) were obtained by using CalcuSyn software for dose effect analysis.⁴⁵

Preliminarily, the solubility and stability of the tested compounds were evaluated. They are soluble in a DMSO/H₂O 1% mixture and proved to be stable under the same experimental conditions of the enzymatic assay.

Supplementary data

Supplementary data associated with this article can be found, in the online version, at [doi:10.1016/j.bmc.2008.04.072](https://doi.org/10.1016/j.bmc.2008.04.072).

References and notes

- Hanefeld, M.; Fischer, S.; Julius, U.; Schulze, J.; Schwanebeck, U.; Schmechel, H.; Ziegelasch, H. J.; Lindner, J. *Diabetologia* **1996**, *39*, 1577.
- Molitch, M. E.; DeFronzo, R. A.; Franz, M. J.; Keane, W. F.; Mogensen, C. E.; Parving, H. H. *Diabetes Care* **2003**, *26*(Suppl. 1), S94.
- Viberti, G. J. *Diabetes Complications* **2005**, *19*, 168.
- Brownlee, M. *Nature* **2001**, *414*, 813.
- Sheetz, M. J.; King, G. L. *JAMA* **2002**, *288*, 2579.
- Eastman, R. C.; Siebert, C. W.; Harris, M.; Golden, P. J. *Clin. Endocrinol. Metab.* **1993**, *77*, 1105.
- Wild, S.; Roglic, G.; Green, A.; Sicree, R.; King, H. *Diabetes Care* **2004**, *27*, 1047.
- Yabe-Nishimura, C. *Pharmacol. Rev.* **1998**, *50*, 21.
- Srivastava, S. K.; Ramana, K. V.; Bhatnagar, A. *Endocr. Rev.* **2005**, *26*, 380.
- Oyama, T.; Miyasita, Y.; Watanabe, H.; Shirai, K. *Diabetes Res. Clin. Pract.* **2006**, *73*, 227.
- Dixit, B. L.; Balendiran, G. K.; Watowich, S. J.; Srivastava, S.; Ramana, K. V.; Petrash, J. M.; Bhatnagar, A.; Srivastava, S. K. *J. Biol. Chem.* **2000**, *275*, 21587.
- (a) Ramana, K. V.; Friedrich, B.; Srivastava, S.; Bhatnagar, A.; Srivastava, S. K. *Diabetes* **2004**, *53*, 2910; (b) Ramana, K. V.; Friedrich, B.; Tammali, R.; West, M. B.; Bhatnagar, A.; Srivastava, S. K. *Diabetes* **2005**, *54*, 818.
- Ramana, K. V.; Srivastava, S. K. *Cytokine* **2006**, *36*, 115.
- Costantino, L.; Rastelli, G.; Cignarella, G.; Vianello, P.; Barlocco, D. *Exp. Opin. Ther. Patents* **1997**, *7*, 843.
- Suzen, S.; Buyukbingol, E. *Curr. Med. Chem.* **2003**, *10*, 1329.
- Tammali, R.; Ramana, K. V.; Srivastava, S. K. *Cancer Lett.* **2007**, *252*, 299.
- Costantino, L.; Rastelli, G.; Vianello, P.; Cignarella, G.; Barlocco, D. *Med. Res. Rev.* **1999**, *19*, 3.
- Costantino, L.; Rastelli, G.; Gamberini, M. C.; Barlocco, D. *Expert Opin. Ther. Patents* **2000**, *10*, 1245.
- Miyamoto, S. *Chem. Biol. Inform. J.* **2002**, *2*, 74.
- El-Kabbani, O.; Ruiz, F.; Darmanin, C.; Chung, R. P.-T. *Cell. Mol. Life Sci.* **2004**, *61*, 750.
- Castañer, J.; Prous, J. *Drugs Future* **1987**, *12*, 336.
- Hotta, N.; Toyota, T.; Matsuoka, K.; Shigeta, Y.; Kikkawa, R.; Kaneko, T.; Takahashi, A.; Sugimura, K.; Koike, Y.; Ishii, J.; Sukamoto, N. *Diabetes Care* **2001**, *24*, 1776.
- Bruno, G.; Costantino, L.; Curinga, C.; Maccari, R.; Monforte, F.; Nicolò, F.; Ottanà, R.; Vigorita, M. G. *Bioorg. Med. Chem.* **2002**, *10*, 1077.
- Maccari, R.; Ottanà, R.; Curinga, C.; Vigorita, M. G.; Rakowitz, D.; Steindl, T.; Langer, T. *Bioorg. Med. Chem.* **2005**, *13*, 2809.
- Maccari, R.; Ottanà, R.; Ciurleo, R.; Vigorita, M. G.; Rakowitz, D.; Steindl, T.; Langer, T. *Bioorg. Med. Chem. Lett.* **2007**, *17*, 3886.
- Urzhumtsev, A.; Tete-Favier, F.; Mitschler, A.; Barbanton, J.; Barth, P.; Urzhumtseva, L.; Biellmann, J. F.; Podjarny, A.; Moras, D. *Structure* **1997**, *5*, 601.
- El-Kabbani, O.; Wilson, D. K.; Petrash, J. M.; Quiocho, F. A. *Mol. Vis.* **1998**, *4*, 19.
- Lee, Y. S.; Hodoscek, M.; Kador, P. F.; Sugiyama, K. *Chem. Biol. Interact.* **2003**, *143–144*, 307.
- Vanjari, H.; Pande, R. J. *Pharm. Biomed. Anal.* **2003**, *33*, 783.
- (a) Muri, E. M. F.; Nieto, M. J.; Sindelar, R. D.; Williamson, J. S. *Curr. Med. Chem.* **2002**, *9*, 1631; (b) Muri, E. M. F.; Nieto, M. J.; Williamson, J. S. *Med. Chem. Rev.* **2004**, *10*, 385; (c) Leoni, F.; Zaliani, A.; Bertolini, G.; Porro, G.; Pagani, P.; Pozzi, P.; Dona, G.; Fossati, G.; Sozzoni, S.; Azam, T.; Bufler, R.; Fantuzzi, G.; Goncharov, I.; Kim, S. H.; Pomerantz, B. J.; Reznikov, L. L.; Siegmund, B.; Dinarello, C. A.; Mascagni, P. *Proc. Natl. Acad. Sci. U.S.A.* **2002**, *99*, 2995; (d) Clare, B. W.; Scozzafava, A.; Supuran, C. T. *J. Med. Chem.* **2001**, *44*, 2253.

31. Reddy, A. S.; Kumar, M. S.; Reddy, G. R. *Tetrahedron Lett.* **2000**, *41*, 6285.
32. (a) Berman, H. M.; Westbrook, J.; Feng, Z.; Gilliland, G.; Bhat, T. N.; Weissig, H.; Shindyalov, I. N.; Bourne, P. E. *Nucleic Acids Res.* **2000**, *28*, 235; (b) <http://www.rcsb.org/pdb>.
33. Zentgraf, M.; Steuber, H.; Koch, C.; La Motta, C.; Sartini, S.; Sottriffer, C. A.; Klebe, G. *Angew. Chem., Int. Ed. Engl.* **2007**, *46*, 3575.
34. El-Kabbani, O.; Darmanin, C.; Schneider, T. R.; Hazemann, I.; Ruiz, F.; Oka, M.; Joachimiak, A.; Schulze-Briese, C.; Tomizaki, T.; Mitschler, A.; Podjarny, A. *Proteins* **2004**, *55*, 805.
35. Steuber, H.; Zentgraf, M.; Gerlach, C.; Sottriffer, C. A.; Heine, A.; Klebe, G. *J. Mol. Biol.* **2006**, *363*, 174.
36. Van Zandt, M. C.; Jones, M. L.; Gunn, D. E.; Geraci, L. S.; Jones, J. H.; Sawicki, D. R.; Sredy, J.; Jacot, J. L.; Dicioccio, A. T.; Petrova, T.; Mitschler, A.; Podjarny, A. D. *J. Med. Chem.* **2005**, *48*, 3141.
37. Steuber, H.; Zentgraf, M.; La Motta, C.; Sartini, S.; Heine, A.; Klebe, G. *J. Mol. Biol.* **2007**, *369*, 186.
38. Steuber, H.; Zentgraf, M.; Podjarny, A.; Heine, A.; Klebe, G. *J. Mol. Biol.* **2006**, *356*, 45.
39. Marvin Calculator Plugins, <http://www.chemaxon.com>.
40. Sherman, W.; Day, T.; Jacobson, M. P.; Friesner, R. A.; Farid, R. *J. Med. Chem.* **2006**, *49*, 534.
41. *Schrödinger Suite 2007*; Schrödinger, LLC; New York, NY, USA, 2007.
42. (a) Gasteiger, E.; Gattiker, A.; Hoogland, C.; Ivanyi, I.; Appel, R. D.; Bairoch, A. *Nucleic Acids Res.* **2003**, *31*, 3784–3788; (b) <http://expasy.org/>.
43. (a) Wolber, G.; Dornhofer, A.; Langer, T. *J. Comput. Aided. Mol. Des.* **2006**, *20*, 773; (b) Wolber, G.; Langer, T. *J. Chem. Inf. Comput. Sci.* **2005**, *45*, 160; (c) *LigandScout 2.0*; Inte:Ligand GmbH, Vienna, Austria, 2007.
44. Costantino, L.; Rastelli, G.; Vescovini, K.; Cignarella, G.; Vianello, P.; Del Corso, A.; Cappiello, M.; Mura, U.; Barlocco, D. *J. Med. Chem.* **1996**, *39*, 4396.
45. Chou, T. -C.; Hayball, M. P. *CalcuSyn software version 1.1.1.*, Biosoft, Cambridge, UK, 1996.
46. *PyMOL Molecular Graphics System v0.99*, DeLano Scientific, Palo Alto, CA, USA, 2006.